Letters

Universal Integrated Onboard Charger With Model Predictive Current Control for Plug-In EV Charging

Harish Karneddi, *Graduate Student Member, IEEE*, Deepak Ronanki, *Senior Member, IEEE*, and Jose Rodriguez, *Life Fellow, IEEE*

***Abstract*—This letter proposes a new universal integrated onboard charger (IOBC) to achieve a wide output voltage range ranging from 48–450 V for plug-in electric vehicle battery charging applications without employing additional power conversion stages. In addition, a model predictive current control (MPCC) is proposed to accomplish boost and buck operation with inherent seamless mode transitions. The proposed IOBC and the MPCC performance are verified through MATLAB simulations and experimental studies on a dSPACE controller-based laboratory prototype. Finally, the key performance characteristics of the proposed IOBC are comprehensively analyzed and compared with the existing IOBCs.**

***Index Terms*—AC-DC power converters, battery chargers, electric vehicles (EVs), power converters.**

I. Introduction

ELECTRIC vehicles (EVs) are predominantly charged by dedicated onboard chargers, which liberate reliance on offboard chargers [1]. These chargers were placed inside the vehicle and consist of dedicated power converters for charging. However, the power rating of these chargers is limited due to space and weight constraints, resulting in a prolonged charging period [2]. Since the propulsion and charging are not simultaneous in the conductive charging, integrated onboard chargers (IOBCs) can be developed by using the traction converter and/or drive for charging purposes. Thus, these chargers enhance the charger power rating while optimizing space, reducing the cost and weight, and simplifying the EV architecture [3]. However, additional conversion stages and hardware circuits are required to reconfigure the traction system for charging operations.

Received 3 May 2024; revised 22 June 2024; accepted 9 July 2024. Date of publication 16 July 2024; date of current version 12 December 2024. The work of Deepak Ronanki was supported in part by the Science and Engineering Research Board (SERB), in part by the Department of Science and Technology (DST), and in part by the Government of India under startup research Grant (SRG)-SRG/2021/000184. The work of Jose Rodriguez was supported by the ANID through Project FB0008, Project 1210208, and Project 1221293. *(Corresponding author: Deepak Ronanki.)*

Harish Karneddi and Deepak Ronanki are with the Department of Engineering Design, Indian Institute of Technology Madras, Chennai 600036, India (e-mail: ed20d016@smail.iitm.ac.in; dronanki@ieee.org).

Jose Rodriguez is with the Faculty of Engineering, Universidad San Sebastian Santiago, Santiago 8370146, Chile (e-mail: jose.rodriguezp@uss.cl).

Color versions of one or more figures in this article are available at https://doi.org/10.1109/TPEL.2024.3428855.

Digital Object Identifier 10.1109/TPEL.2024.3428855

Several EVs utilize a 3-ϕ permanent magnet synchronous motor (PMSM) drive for propulsion. Thus, researchers proposed several 3-ϕ IOBCs [3]. Nonetheless, most of these IOBCs often cause wear, audible noise, and efficiency issues due to their rotational fields, necessitating a locked rotor during charging. Additionally, a 3-ϕ supply is not commonly available in residence. Consequently, 1-ϕ IOBCs are more popular, and researchers proposed various 1-ϕ IOBCs [4], [5], [6], [7], [8], [9]. A two-channel interleaved boost-converter-based IOBC is introduced using the diode bridge rectifier (DBR) along with the traction system, which results in more losses and is limited to a lower power rating [4]. Bridgeless interleaved boost converter-based IOBCs are introduced in [5] and [6]. In addition, an active power decoupling circuit is incorporated to mitigate the 2nd harmonic ripple in the output voltage [5]. However, these chargers are boost-derived and capable of charging the battery packs, which have a voltage higher than the maximum grid voltage ($V_{g\max}$). A dc-dc boost-buck IOBC is implemented to charge the LV battery pack vehicles [7], although it necessitates an additional front-end rectifier. While boost-buck IOBCs are proposed in [8] and [9], these chargers demand more conversion stages and involve intermediate life-limited dc-link capacitors. Consequently, most of these IOBCs are boost-configured and unable to charge all the EVs from a universal ac supply. While a few wide voltage range IOBCs are realized by using an additional conversion stage, this increases the cost, occupies significant space, adds weight, and degrades the performance.

To overcome these concerns, this letter introduces a new wide output voltage range 1-ϕ universal IOBC to charge the EV's battery voltages ranging from 48–450 V without any additional active/passive components. Nonetheless, the control of the proposed charger imposes significant challenges in attaining seamless mode transition. Several smooth transition-based techniques are proposed to operate in multimode [10]. However, the control degree increases from one duty cycle to two duty cycles. During the transition, some controllers introduce an additional operating mode, i.e., a boost-buck mode [11]. However, these degrade the performance and complex the control design. Furthermore, the linear controllers have current distortion at the zero crossing intervals in the controlled rectifiers owing to the limited gain, resulting in increased grid current total harmonic distortion (THD). To avoid these problems, a model predictive current control (MPCC) is proposed in this letter to regulate the grid current by optimally selecting the switching

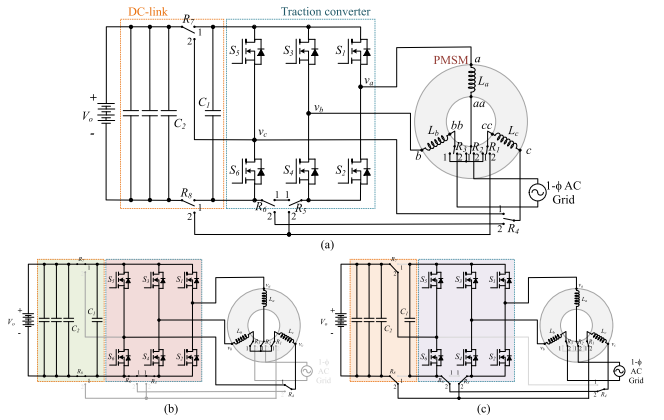

Fig. 1. Proposed universal IOBC: (a) Charger topology. (b) Propulsion mode configuration. (c) Charging mode configuration.

sequence. Furthermore, this control approach will reduce the switching frequency, thereby enhancing the charger efficiency in comparison to the conventional linear control approach.

II. Proposed IOBC and MPCC

A. Proposed IOBC Configuration

The proposed universal IOBC shown in Fig. 1(a) is realized using only the traction converter and drive winding; eight relays ($R_1 - R_8$) are used to reconfigure the existing traction system for propulsion and charging operations. During propulsion, these relays are set to position-1, configuring them as a typical traction drive system, as depicted in Fig. 1(b). Conversely, the relays are set toward position-2 to realize the proposed wide voltage range IOBC during charging, as illustrated in Fig. 1(c). The operating mode of the proposed IOBC is contingent on the EV battery voltage (V_o) and the grid voltage ($v_g(t)$). During $V_o > |v_g(t)|$, the charger operated in boost mode; otherwise, the charger operated in buck mode. The proposed IOBC consists of three pairs of switches ($S_1 - S_2$, $S_3 - S_4$, and $S_5 - S_6$) and is operated in complementary, resulting in $2^3 = 8$ potential switching states during the charging, as listed in Table I. The charger's operating switching state is controlled to attain a wide voltage range of operation.

B. Criteria for Zero Torque Production During Charging

Since the traction motor windings are used for charging purposes in IOBCs, there is a chance of torque production during charging mode. Understanding the conditions under which zero torque is generated during charging is crucial for IOBCs. Torque production can be analyzed on a per-phase basis using co-energy considerations derived from the stationary frame model of the traction motor [12]. The torque contribution of each phase can be expressed as follows:

$$\tau_x = \frac{i_x^2}{2}\frac{dL_x}{d\theta} + i_x\frac{d\psi_f}{d\theta} \tag{1}$$

where ψ_f, τ_x, i_x, and L_x are the magnetic flux of the permanent magnet (rotor flux linkage), torque production by x-phase, x-phase current, and inductance of the x-phase, respectively, ($x \in \{a, b, c\}$). The torque contribution of each phase can be determined as follows:

TABLE I
Switching States of the Proposed IOBC

Grid voltage	State (j)	$S_1 = \overline{S_2}$	$S_3 = \overline{S_4}$	$S_5 = \overline{S_6}$	v_{ab}
$v_g(t) > 0$	1	0	0	1	0
	2	1	0	1	V_o
	3	1	0	0	$V_o - v_{C_1}$
	4	0	0	0	0
$v_g(t) < 0$	5	1	1	1	0
	6	0	1	1	V_o
	7	0	1	0	$V_o - v_{C_1}$
	8	1	1	0	0

$v_g(t)$: grid voltage, V_o: output voltage, and v_{c_1}: voltage across C_1, respectively.

$$\tau_a = i_a^2(L_q - L_d)\sin 2\theta - i_a\psi_f \sin(\theta) \tag{2}$$

$$\tau_b = i_b^2(L_q - L_d)\sin 2\left(\theta - \frac{2\pi}{3}\right) - i_b\psi_f \sin\left(\theta - \frac{2\pi}{3}\right) \tag{3}$$

$$\tau_c = i_c^2(L_q - L_d)\sin 2\left(\theta + \frac{2\pi}{3}\right) - i_c\psi_f \sin\left(\theta + \frac{2\pi}{3}\right) \tag{4}$$

where, ψ_f, L_d, L_q, θ, τ_a, τ_b, τ_c, i_a, i_b, and i_c are the rotor flux linkage, d-axis inductance, q-axis inductance, mechanical angle/rotor position and the torques produced by a, b, and c phases, and the current through a, b and c windings, respectively. During the charging mode of the proposed charger, a-phase and b-phases are connected at the grid side, as depicted in Fig. 1(c). These windings carry the same magnitude of currents but are out of phase, i.e., $i_a = -i_b = i_g$. The buck arm assists the output filter while operating in the boost mode, resulting in approximately zero average current through the c-phase winding ($\tau_c \approx 0$). The total torque (τ_{total}) production by the currents through the remaining two phases can be expressed as follows:

$$\tau_{\text{total}} = i_g^2(L_q - L_d)\sin\left(2\theta + \frac{\pi}{3}\right) - \sqrt{3}i_g\psi_f \sin\left(\theta + \frac{\pi}{6}\right) \tag{5}$$

The torque (5) demonstrates that the torque production can be eliminated by adjusting the rotor position, i.e., torque production is zero for $\theta = (n\pi - \frac{\pi}{6})$, where $n \epsilon \{0, 1, 2, .., \infty\}$. Therefore, the traction motor's position must be adjusted before operating in charging mode for zero torque production during charging. On the other hand, the c-phase carries a nonzero dc current while operating in buck mode of operation and may cause the demagnetization of the rotor magnetic field. Thus, the c-phase winding has to connect in such a way that the current through this phase forms an electromagnetic pole, which has to be coupled magnetically with the rotor's permanent magnetic poles. It results in approximately zero-torque production and avoids demagnetization during charging mode.

C. Proposed Predictive Control

A new dual-loop control architecture is proposed with an inherent seamless transition for the wide voltage range of IOBC. The outer loop is a current/voltage loop and is realized with a linear controller that monitors the charging current/voltage (I_o/V_o) and generates the reference grid current ($i_g{}^*(t)$). The inner loop is realized with the MPCC algorithm, which generates the switching pulses from $i_g{}^*(t)$, actual grid current ($i_g(t)$),

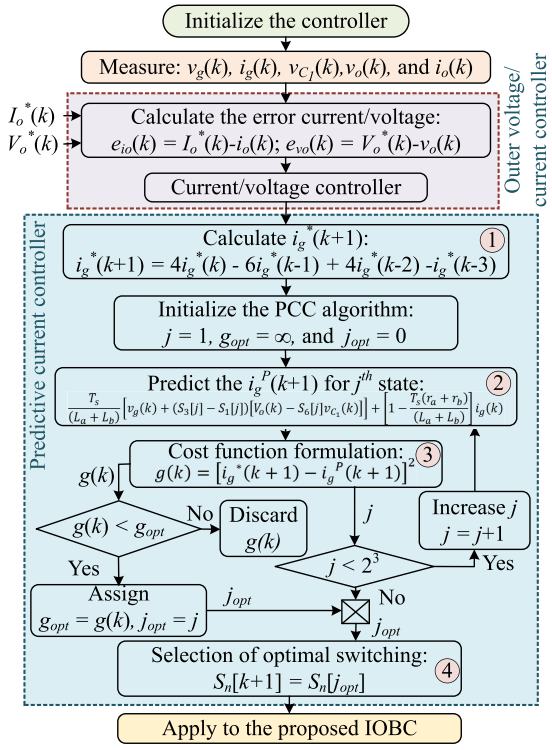

Fig. 2. Flow chart of the proposed MPCC for a wide voltage-range IOBC.

and the proposed charger model. The design algorithm of the proposed MPCC is shown in Fig. 2, and the same is described as follows.

1) The outer loop computes the reference current at the kth sample, i.e., $i_g{}^*(k)$. However, it is mandated to compare the reference grid current and the predicted grid current at $(k+1)$th sample to predict the switching state for $(k+1)$th state. Thus, the $i_g{}^*(k+1)$ can be determined using Lagrange extrapolation [13] as follows:

$$i_g{}^*(k+1) = 4i_g{}^*(k) - 6i_g{}^*(k-1) + 4i_g{}^*(k-2) - i_g{}^*(k-3) \quad (6)$$

2) The $i_g{}^P(k+1)$ corresponding to jth state ($j \in (1-8)$) can be predicted using the modeling equation of the proposed IOBC, corresponding switching states, and kth state feedbacks and it is expressed as follows:

$$i_g^P(k+1) = \alpha\,[v_g(k) - v_{ab}(k)] + \beta i_g(k)$$
$$\alpha = \frac{T_s}{(L_a+L_b)}; \quad \beta = \left[1 - \frac{2T_s(r_a+r_b))}{(L_a+L_b)}\right] \quad (7)$$

$$v_{ab}(k) = (|S_1 - S_3|)\,[v_o(k) - S_6 v_{C_1}(k)] \quad (8)$$

where, T_S, L_a, L_b, r_a, and r_b, are the sampling time, phase-a and phase-b inductance and resistances, respectively.

3) The cost function ($g(k)$) is formulated with extrapolated reference grid current ($i_g{}^*(k+1)$) and predicted grid current ($i_g{}^P(k+1)$) at all potential switching states as follows:

$$g(k) = \left[i_g{}^*(k+1) - i_g{}^P(k+1)\right]^2 \quad (9)$$

TABLE II
DESIGN SPECIFICATIONS OF THE PROPOSED IOBC

Specifications of the IOBC		Component values	
Parameters	Rating	Component	Rating
Input voltage	85–265 V	min. $L_a = L_b$	0.55 mH
Input frequency	50/60 Hz ± 1%	min. L_c	0.42 mH
Power rating	3.3 kW	C_1	44 F
Current ripple	20%	C_2	0.94 mF
Voltage ripple	10%	Holding time (t_{hold})	20 ms
Sampling time	20 µs	Battery voltage (V_o)	48-450 V

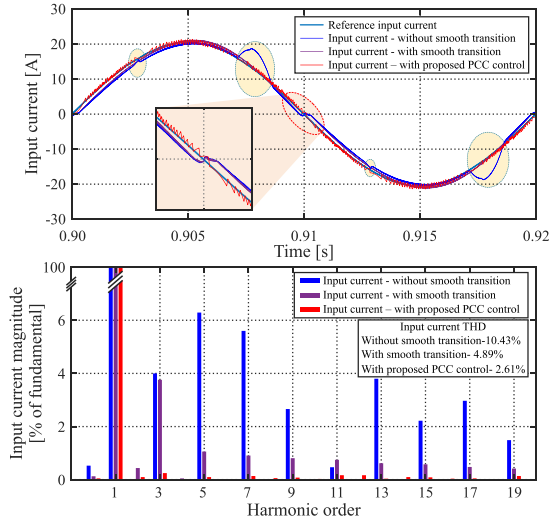

Fig. 3. Performance of the proposed IOBC with different controls.

4) The switching state corresponding to the minimal cost function among all the switching states ($S_n[j_{\text{opt}}]$) is the optimal switching state (j_{opt}) for the $(k+1)$th sampling interval. The same is chosen as the switching state for $(k+1)$th sampling instant and is applied to the proposed IOBC.

III. RESULTS AND DISCUSSION

A 3.3 kW charger is developed to assess the efficacy of the proposed universal IOBC with the MPCC. The design specification and accompanying component ratings are listed in Table II. A constant current–constant voltage (CC-CV) charging technique is adopted to charge the EV battery. An MPCC is implemented to attain the desired performance by adhering to the design steps. The outer current and voltage loops are realized with the proportional–integral (PI) controller with a lower bandwidth to attenuate the 2nd harmonic ripple. The proposed IOBC is fed with a 1-ϕ, 230 V, 50 Hz ac supply, and a CV charging mode is considered to assess the wide-range operation of the proposed IOBC.

During the 250 V battery pack charging, the proposed IOBC operated in boost mode (250 V$>v_g(t)$) and buck mode (250 V$<v_g(t)$), subjected to the periodic mode transition. The performance of the proposed IOBC without smooth transition, with a smooth transition-based conventional linear control, and proposed MPCC, is illustrated in Fig. 3. Without smooth transition-based control, current spikes appear at mode transitions, resulting in the presence of dominating lower

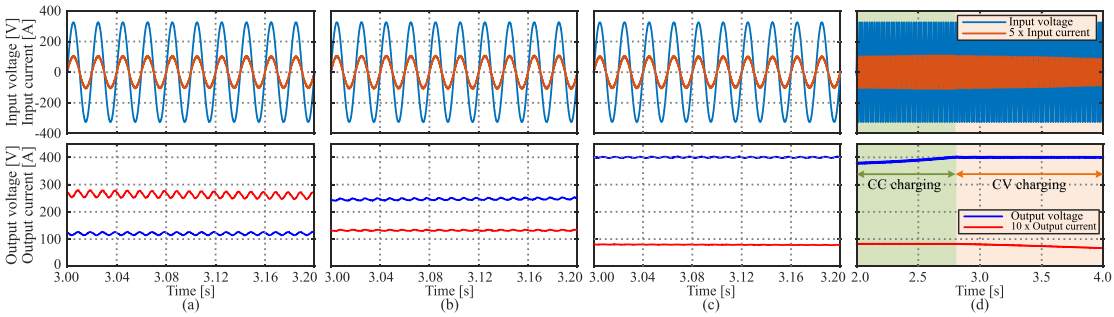

Fig. 4. Simulation results of the proposed IOBC for V_o^* (a) 120 V, (b) 250 V, (c) 400 V, and (d) 400 V CC–CV charging mode.

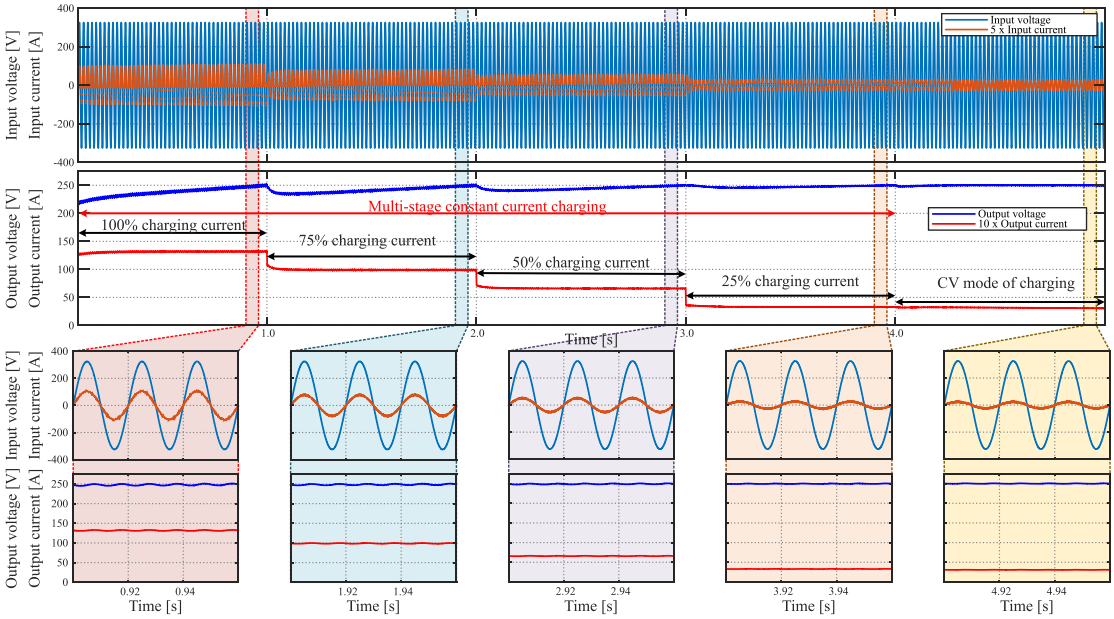

Fig. 5. Performance of the proposed IOBC under rapid charging scenarios.

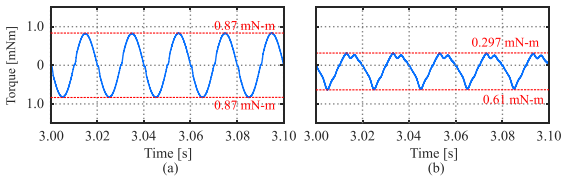

Fig. 6. Torque production during (a) 400 V charging and (b) 250 V charging (Base torque of the motor is 23.74 N m).

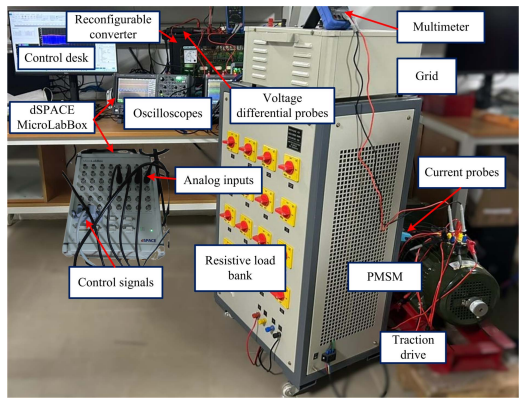

Fig. 7. Test-setup platform of the proposed IOBC.

order harmonics in the grid current. Meanwhile, the conventional smooth transition-based control attains a seamless mode transition; however, a zero crossing distortion is presented in Fig. 3. Conversely, the proposed MPCC also contains zero-crossing distortion. Moreover, the impact of this distortion is very low due to the superior dynamic performance and the variable switching frequency. After a zero-crossing instant, the proposed charger, along with the MPCC, operates continuously on the rising slope and quickly tracks the reference grid current. As a result, the MPCC improves the charger's performance during zero-crossing instants and maintains the grid current closer to the reference current while ensuring a seamless transition. Furthermore, the performance of the proposed IOBCs at a wide voltage range of operation is shown in Fig. 4. In addition, the performance of the proposed IOBC under rapid charging scenarios was evaluated using the multistage CC–CV (MSCC–CV) charging technique while charging a 250 V battery. The results are illustrated in Fig. 5, demonstrating that the proposed charger operates satisfactorily during these rapid charging conditions. Fig. 6 shows the torque production of the traction motor while charging the 400 V and 250 V battery packs. During these modes, the proposed charger produces 0.9 and 0.61 mN m peak

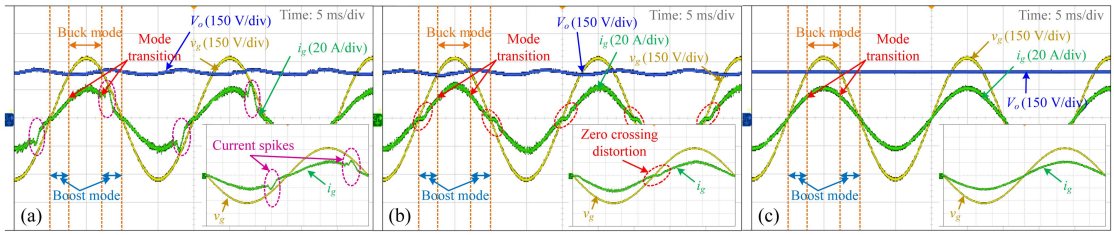

Fig. 8. Experimental performance studies of the proposed IOBC while charging 250 V battery: Conventional linear control (a) without seamless transition, (b) with seamless transition, and (c) proposed MPCC.

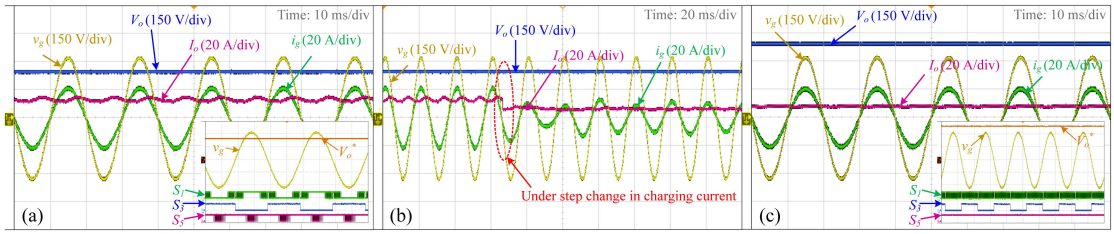

Fig. 9. Test results of the proposed IOBC: 250 V charging: (a) Steady-state performance. (b) Dynamic performance. (c) 400 V steady-state performance.

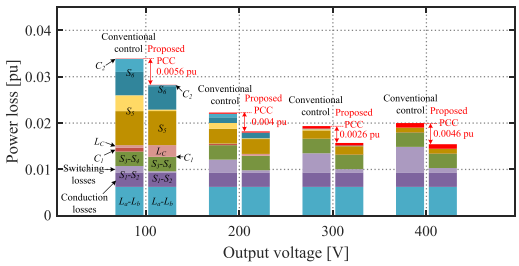

Fig. 10. Loss distribution of the proposed IOBC with conventional linear and proposed MPCC controls.

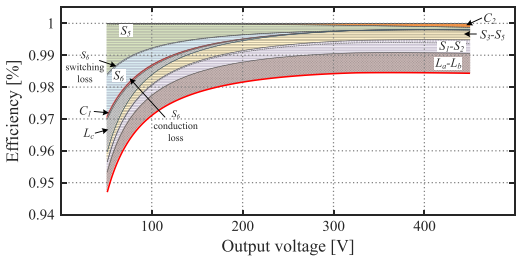

Fig. 11. Efficiency of the proposed IOBC under wide battery pack voltages.

TABLE III
PERFORMANCE STUDIES OF THE PROPOSED IOBC

Output	Conventional control		Proposed MPCC	
voltage [V_o]	i_g THD [%]	Power factor	i_g THD [%]	Power factor
48 V	5.47	0.9985	2.02	0.9997
120 V	4.96	0.9987	1.89	0.9998
250 V	4.89	0.9988	2.61	0.9996
400 V	3.72	0.9993	3.50	0.9993

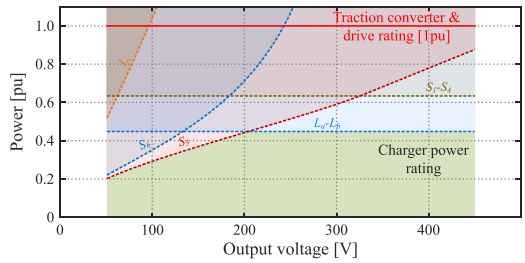

Fig. 12. Possible charger power rating of the proposed IOBC in terms of traction system power ratings.

torques, which are significantly less than the traction motor's base torque (24.73 N m). Therefore, the torque generated during the charging mode at all operating conditions is considered to be negligible.

A laboratory prototype of the proposed IOBC is designed with a 3-ϕ PMSM and three-leg reconfigurable converter, as depicted in Fig. 7. A 1-ϕ autotransformer is used as an input power supply during charging mode, and the battery is realized with its equivalent resistive load. The controller is implemented on a dSPACE MicroLabBox. The experimental results of a proposed IOBC without smooth transition-based control, with a conventional smooth transition-based control, and with proposed MPCC are illustrated in Fig. 8. The proposed MPCC preserves seamless mode transition and has a negligible zero crossing distortion. The steady-state and dynamic performance of the proposed IOBC with the MPCC while operating with 250 and 400 V output voltages are illustrated in Fig. 9. In both 250 V [see Fig. 9(a)] charging and 400 V battery pack charging [see Fig. 9(c)], the proposed charger and its controller maintained the desired battery voltage with allowable voltage ripple. To assess the dynamic performance of the controller, the studies are performed during a step change in charging current during 250 V battery pack charging and their performance is shown in Fig. 9(b). The controller shows better dynamic performance and brings the charger into steady-state operation quickly.

TABLE IV
COMPARISON OF THE PROPOSED IOBC WITH EXISTING 1-ϕ IOBCS

	Ref. [4]	Ref. [5]	Ref. [6]	Ref. [7]	Ref. [8]	Ref. [9]	Proposed IOBC
Input supply	1-ϕ, 90-240 V, 50 Hz	1-ϕ, 220 V, 50 Hz	1-ϕ, 220 V, 50 Hz	DC, 260 V	1-ϕ, 110 V, 60 Hz	1-ϕ, 90-115 V, 60 Hz	1-ϕ, 85-265 V, 50/60 Hz
Charger configuration	DBR followed by interleaved boost	Bridgeless boost with APD	Bridgeless interleaved boost	SBC followed by interleaved boost converter	Interleaved boost followed by buck converter	3-leg interleaved boost followed by dc-dc converter	Proposed boost-buck converter
No. of switches	6	6	6	8	14	12	6
No. of diodes	6	0	0	0	0	0	0
No. of relays	2	5	2	2	2	2	8
Additional converters	DBR	–	–	SBC	–	Dc-dc converter	–
Battery voltage	340-420 V	400 V	400 V	230 V	250 V	400 V	48-450 V
Operating mode	Boost mode	Boost mode	Boost mode	Buck-boost mode	Boost-buck mode	Boost-buck mode	Boost-buck mode
Control	Dual loop linear control	Dual loop predictive control	Dual loop linear control	Different buck and boost linear controls	Different buck and boost with PR controls	Two distinct dual loop linear control	Proposed MPCC
V2G compatibility	No	Yes	Yes	Yes	Yes	Yes	Yes
Inherent smooth transition	Not required	Not required	Not required	Two distinct conversion stages	Two distinct conversion stages	Two distinct conversion stages	Yes

APD: active power decoupling, DBR: diode bridge rectifier, SBC: synchronous buck converter, and PR: proportional-resonant, respectively.

Furthermore, the power loss distribution of the proposed IOBC with conventional smooth-transition control and proposed MPCC is depicted in Fig. 10. The proposed charger, along with the MPCC control, exhibits better performance in comparison to the conventional control. The efficiency and loss distribution of the proposed charger over a wide voltage range operation is depicted in Fig. 11. Compared to high-voltage charging, the proposed charger has a comparatively lower efficiency when operating at low voltage. In addition, the performance characteristics, such as grid current THD and power factor at wide voltage, are presented in Table III,which comply with the IEEE 519:2014 standards. The main concern with the IOBC is that the traction system's power rating limits its power rating and directly implies the charger's fast charging capability. In addition, the device amperage of the proposed IOBC varies with the output voltage. Hence, it is crucial to analyze the power constraints of the proposed IOBC at a wide output voltage range based on the active and passive components. Thus, studies are performed to determine the potential power rating of the proposed IOBC. Fig. 12 shows the possible power rating of the proposed charger on the basis of traction system power rating and its constraints. Finally, the distinguishing features of the proposed IOBC are compared with the existing IOBCs and are summarized in Table IV.

IV. CONCLUSION

This letter proposed a new universal IOBC to charge an EV having battery voltages ranging from 48–450 V. In addition, an MPCC is introduced to accomplish a wide voltage range operation with an inherent seamless mode transition. The simulation and experimental results demonstrate that the proposed IOBC, along with MPCC, preserves the desired charging current/voltage at the output with negligible ripple. In addition, the proposed MPCC control maintains the sinusoidal current in phase with the grid voltage and has an inherent smooth mode transition along with negligible zero-crossing distortion. While charging 48–450 V battery packs, the proposed charger with MPCC complies with IEEE 519:2014 and IEC 61000-3-2 standards. The proposed charger with the MPCC control has operated with comparatively greater efficiency than the conventional linear control. The maximum power rating of 44% of the traction system is possible with the proposed universal IOBC, and the same can be enhanced up to 64% of traction power. Thus, the proposed IOBC is an elegant solution for universal plug-in EV charging applications.

REFERENCES

[1] H. Wouters and W. Martinez, "Bidirectional onboard chargers for electric vehicles: State-of-the-art and future trends," *IEEE Trans. Power Electron.*, vol. 39, no. 1, pp. 693–716, Jan. 2024.

[2] D. Ronanki and H. Karneddi, "Electric vehicle charging infrastructure: Review, cyber security considerations, potential impacts, countermeasures, and future trends," *IEEE J. Emerg. Sel. Topics Power Electron.*, vol. 12, no. 1, pp. 242–256, Feb. 2024.

[3] A. Khaligh and M. D'Antonio, "Global trends in high-power on-board chargers for electric vehicles," *IEEE Trans. Veh. Technol.*, vol. 68, no. 4, pp. 3306–3324, Apr. 2019.

[4] C. Shi, Y. Tang, and A. Khaligh, "A single-phase integrated onboard battery charger using propulsion system for plug-in electric vehicles," *IEEE Trans. Veh. Technol.*, vol. 66, no. 12, pp. 10 899–10 910, Dec. 2017.

[5] D. Bhule and R. S. Kaarthik, "A model predictive control scheme for a single-phase integrated battery charger with active power decoupling for EV application," *IEEE Trans. Power Electron.*, vol. 39, no. 4, pp. 4117–4126, Apr. 2024.

[6] J. Gao, W. Sun, D. Jiang, Y. Zhang, and R. Qu, "Improved operation and control of single-phase integrated on-board charger system," *IEEE Trans. Power Electron.*, vol. 36, no. 4, pp. 4752–4765, Apr. 2021.

[7] C. Viana and P. W. Lehn, "A drivetrain integrated DC fast charger with buck and boost functionality and simultaneous drive/charge capability," *IEEE Trans. Transport. Electrific.*, vol. 5, no. 4, pp. 903–911, Dec. 2019.

[8] S. He, Z. Xu, M. Chen, H. Yang, and W. Li, "General derivation law with torque-free achieving of integral on-board charger on compact powertrains," *IEEE Trans. Ind. Electron.*, vol. 68, no. 2, pp. 1791–1802, Feb. 2021.

[9] M. Z. Farooqi, B. Singh, and B. K. Panigrahi, "Enhanced control and modulation of on-board integrated EV charger with active power decoupling capability," *IEEE Trans. Transport. Electrific.*, early access, Mar. 25, 2024, doi: 10.1109/TTE.2024.3381607.

[10] K.-C. Wu, H.-H. Wu, and C.-L. Wei, "Analysis and design of mixed-mode operation for noninverting buck–boost DC–DC converters," *IEEE Trans. Circuits Sys. II: Exp. Briefs*, vol. 62, no. 12, pp. 1194–1198, Dec. 2015.

[11] L. Callegaro, M. Ciobotaru, D. J. Pagano, E. Turano, and J. E. Fletcher, "A simple smooth transition technique for the noninverting buck–boost converter," *IEEE Trans. Power Electron.*, vol. 33, no. 6, pp. 4906–4915, Jun. 2018.

[12] P. C. Krause, O. Wasynczuk, S. D. Sudhoff, and S. Pekarek, *Analysis of Electric Machinery and Drive Systems*. Hoboken, NJ, USA: Wiley, 2013.

[13] V. Yaramasu and B. Wu, *Model Predictive Control of Wind Energy Conversion Systems*. Hoboken, NJ, USA, Wiley-IEEE Press, 2017.